EURASIP Journal on Advances in Signal Processing

RESEARCH Open Access

Wavelet analysis on a generalized helix space curves and its examples

Xiaohui Zhou[1*]

*Correspondence:
zhou001900@163.com

[1] Shanghai University of Finance and Economics-Zhejiang College, Jinhua 321000, Zhejiang, China

Abstract

In this paper, wavelet transform on a generalized helix space curves are investigated, including of local continuous wavelet transform at some point and discrete wavelet transform on a class of helix curves. Firstly, a class of helix space curves are introduced and the parameter equations are given. Then the dilation operator and translation on the function $\psi^{(\xi_0)}$ is properly defined by the local projection at some point from a space curve on the unit sphere onto its tangent line. The local continuous wavelet transform and its reconstruction formula are deduced at some point of a space curve on the unit sphere. On the other hand, According to the discretization of length-preserving projection, discrete wavelet transform is lifted onto a helix space curve, such as a circular helix curve. Based on length-preserving projection, the some properties are discussed, such as two-scale sequences of scaling function and wavelet, orthogonality, decomposition formula and so on. Finally, two examples are given for our discussion. One example is illustrating the application of local continuous wavelet transform at some point of a space curve. The result shows the signal at some point of a space curve can be reconstructed by local continuous wavelet method. The norm of the error is 0.3783 between original signal and reconstructed signal in this example. The other numerical example is given for decomposing and reconstructing with the signal on a circular helix curve. The result shows the signal on a helix space curve can be decomposed and reconstructed by the length-preserving projection. The norm of the error is 8.0741×10^{-11} between original signal and reconstructed signal. The figures are shown for the simulation results.

Keyword: Discretization of length-preserving projection, Helix space curves, Tangent projection

1 Introduction

In recent years, the development of wavelet method is rapid and profound. It can process non-stationary data, localize in time domain, and perform multi-scale analysis of signals. Wavelet analysis is widely applied in many fields, such as signal processing, the image denoising, object detection [1], facial biometrics [2], medicine (some organs are regarded as sphere-like surfaces), financial data [3–6] and so on. Some data in the real world may be involved in a particular smooth manifold, such as the two-sheeted

hyperboloid, the paraboloid; or other various two-dimensional smooth manifolds; and various abstract manifolds. One feasible method to study the wavelet on a manifold is based on Lie groups, Lie algebras, and its representation theory. For example, Leduc discussed continuous spatiotemporal wavelet transform by unitary representation of the kinematical Group [7]. Continuous spatiotemporal wavelet is widely used for missile warhead detection [8] and tracking; analysis of multi-scale phenomena in geophysical [9, 10], a particular form of a stochastic wavelets [7] and so on. Another feasible method to discuss the wavelet and its application on a manifold [11] is by using bijective projection, such as the vertical projection, the radial projection, stereographic projection, area-preserving projection, length-preserving projection and so on. Based on the wavelet method on a particular curve, some new interpretation are presented in dealing with financial data (bitcoin transaction data, data of deposit balances of financial institutions and so on), such as 'volatility on regression growth trend', 'error on regression growth trend', 'wavelet approximate data on the regression trend line' and so on [5, 6]. These financial data processing are mainly on a plane curve, such as a linear regression curve [5], a logarithm curve and so on. Moreover, many data in the real world may be in some space curves, such as flight data, satellite orbit data, biology (DNA double helix structure) and so on. For example, seismic data form a spatial curve on the earth's surface. Taking wavelet transform on this kind of data is a useful example of the wavelet analysis on the spatial curve. The seismic data was decomposed into three levels by DWT to construct the linear response spectrum of single degrees of freedom (SDOF) systems under the main and decomposed earthquakes [17]. Moreover, Kamgar et al. [18, 19] proposed an innovative method to reduce the computational volume and time of NDA by discrete wavelet transform. Several far- and near-field ground motion records are selected and decomposed into three levels by Wavelet Db4. Then, several single-degree-of-freedom systems are generated and modeled by OpenSees with different beam-to-column stiffness ratios. Heidari et al. [20] investigated a method by DWT, select far-field near-field ground motion data and decompose it into three levels to reduce the quantity and time. In the work, Strong Ground Motion (SGM) parameters are calculated in different kinds of soil with different magnitudes by DWT. The Main Earthquake Record (MER) is divided into approximation and detailed signals by wavelet denoising. The high and low frequencies of MER are separated from each other. These data may be on a space or a surface which is on a sphere. The wavelet method should be generated onto a space curves. In this paper, wavelet analysis is discussed for dealing with some data on a class of space curves. Two cases are discussed respectively. The first is the continuous wavelet transform at an interval of a point on a spherical space curve. In this case, we compute the Frenet frame of a local point on the spherical space curve, the continuous wavelet transform and inverse transform of the local point. This provides the basis for the approximate wavelet analysis of local points in later studies. The second is to discuss the discretized wavelet transformation and reconstruction on the circular helix curve by the Euler discretization scheme of a spatial curve. This is a discretization method that can flatten the spatial curve approximatively.

This paper will be organized as follows: In Sect. 2, the preliminaries are introduced, such as definitions of a class of helix space curves, local bijection projection on a space curve and so on. In Sect. 3, local continuous wavelet transform on a space curve on a

unit sphere is discussed by local bijection projection and the local dilation. Moreover, the reconstruction formula is also obtained. In Sect. 4, discrete wavelet transform is lifted onto a helix space curve by length-preserving projection, including of scaling function and wavelet on a helix space curves, decomposition and reconstruction on a helix space curve. Finally, two examples are given for our discussion. One example is illustrating the application of local continuous wavelet transform at some point of a space curve on a unit sphere. The other numerical example is given for decomposing and reconstructing with the signal on a circular helix curve. The figures are shown for the simulation results.

2 Preliminary

In this section, we introduce a class of helix space curves, local bijection projection and other concepts.

2.1 The equations of helix space curves

The equation of a circular helix is given by the following movement. It is known to all that a particle around a fixed axis to do a uniform circular movement and move with a constant speed parallelly to the axis. Its trajectory is a cylindrical helix. The equation is as follows:

$$\vec{r} = \{u\cos(v), u\sin(v), av\}.$$

If the movement with a constant speed parallel to the axis is changed to another circular motion in the above motion. That means a particle around a fixed axis to do a uniform circular movement and do another circular movement with a constant speed, such as a satellite moving around the earth and also around the sun. Its trajectory is a circular helix. The equation is given in the following definitions.

Definition 2.1 If the trajectory of a prime point satisfies the following parameter equation:

$$\vec{r} = \{(a + v_0\cos(\omega t))\cos(t), (a + v_0\cos(\omega t))\sin(t), v_0\sin(\omega t)\} \tag{1}$$

where $|v_0| < a$, a, v_0 denotes the radius of two circular motions, ω is the angular speed, then the trajectory is a circular helix.

If the circle parallel to the XOY plane becomes an elliptic in the above equation, the trajectory equation can be obtained in Definition 2.2.

Definition 2.2 If the trajectory of a prime point satisfies the following parameter equation:

$$\vec{r} = \{(a + v_0\cos(\omega t))\sec(t), (b + v_0\cos(\omega t))\tan(t), v_0\sin(\omega t)\} \tag{2}$$

where $|v_0| < a$, a, b are the long half axis and the short half axis of an ellipse and v_0 denotes the radius of the circle, ω is the angular speed, then the trajectory is a elliptic helix.

Generalizing the Definitions 2.1 and 2.2, we have

Definition 2.3 For a continuous plane guide curve F(x,y) = 0, its parameter equation is

$\begin{cases} x = f(t) \\ y = g(t) \end{cases}$, t is a parameter.

Then the general equation of a generalized helix is

$$\vec{r} = \{(a + v_0 \cos(\omega t))f(t), (a + v_0 \cos(\omega t))g(t), v_0 \sin(\omega t)\} \tag{3}$$

where a, v_0, ω are constants satisfying some conditions.

Next, two examples are given for showing the adjacent structure of a point on a generalized helix. For the equation of a generalized helix,

$$\vec{r} = \{(a + v_0 \cos(\omega t))f(t), (a + v_0 \cos(\omega t))g(t), v_0 \sin(\omega t)\},$$

The following derivative can be obtained that by simple computation.

$$\vec{r'} = \{(a+v_0 \cos(\omega t))f'(t) - \omega v_0 \sin(\omega t)f(t), (a+v_0 \cos(\omega t))g'(t) - \omega v_0 \sin(\omega t)g(t), v_0\omega \cos(\omega t)\}$$

$$\begin{aligned}\vec{r''} = \Big\{&(a + v_0 \cos(\omega t))f''(t) - 2\omega v_0 \sin(\omega t)f'(t) - \omega^2 v_0 \cos(\omega t)f(t), (a + v_0 \cos(\omega t))g''(t) \\ &-2\omega v_0 \sin(\omega t)g'(t) - \omega^2 v_0 \cos(\omega t)g(t), -v_0\omega^2 \sin(\omega t)\Big\}\end{aligned}$$

Moreover,

$$\begin{aligned}\vec{r'} \times \vec{r''} = \Big\{&\omega^3 v_0^2 g(t) - g''(t)\omega v_0 \cos(\omega t)(a + v_0 \cos(\omega t)) + \omega^2 v_0 \sin(\omega t)g'(t)(v_0 \cos(\omega t) - a), \\ &- \omega^3 v_0^2 f(t) + f''(t)\omega v_0 \cos(\omega t)(a + v_0 \cos(\omega t)) - \omega^2 v_0 \sin(\omega t)f'(t)(v_0 \cos(\omega t) - a), \\ &(a + v_0 \cos(\omega t))^2(f'(t)g''(t) - g'(t)f''(t)) - \omega v_0 \sin(\omega t)(a + v_0 \cos(\omega t))(f(t)g''(t) - g(t)f''(t)) \\ &- \left[\omega^2 v_0 \cos(\omega t)(a + v_0 \cos(\omega t)) + 2\omega^2 v_0^2 \sin^2(\omega t)\right](f'(t)g(t) - g'(t)f(t))\Big\}.\end{aligned}$$

The Frenet frame can be established by the following vectors:

$$\vec{\alpha} = \frac{\vec{r'}}{\left|\vec{r'}\right|}, \vec{\gamma} = \frac{\vec{r'} \times \vec{r''}}{\left|\vec{r'} \times \vec{r''}\right|}, \vec{\beta} = \vec{\gamma} \times \vec{\alpha}. \tag{4}$$

Example 2.1 Choose the parameters $a = 0, v_0 = 1, \omega = 1$ and the function $f(t) = \cos t$, $g(t) = \sin t$ in Eq. (3). Then the parameter equation of a space curve is rewritten as follows:

$$\vec{r} = \{\cos(t) \cos t, \cos(t) \sin t, \sin(t)\}$$

It is easy to be identified that this space curve is on the unit sphere. Its figure is shown in Fig. 1. By computing simply, its tangent vector is

$$\vec{r'} = \{-\sin 2t, \cos 2t, \cos(t)\} \tag{5}$$

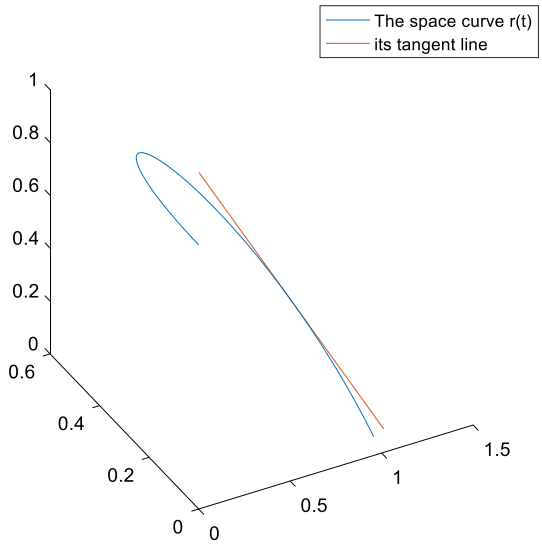

Fig. 1 A space curve and its tangent line on a unit ball

Since $\vec{r}(t_0) \cdot \vec{r'}(t_0) = 0$, for every point t_0, $\vec{r}(t_0)$ is vertical with $\vec{r'}(t_0)$, that means $\vec{r}(t_0) \perp \vec{r'}(t_0)$. Choose the point $t_0 = \frac{\pi}{10}$ and compute its tangent vector by Eq. (4). The figure of its tangent line at point $t_0 = \frac{\pi}{10}$ is shown by the red line in Fig. 1. Moreover, The Frenet frame at point $t_0 = \frac{\pi}{10}$ can be established by computing Eq. (4). By computing the curvature κ_0 and scratch rate τ_0 at point $t_0 = \frac{\pi}{10}$, the space coordinate (x, y, z) of the adjacent points can be denoted by

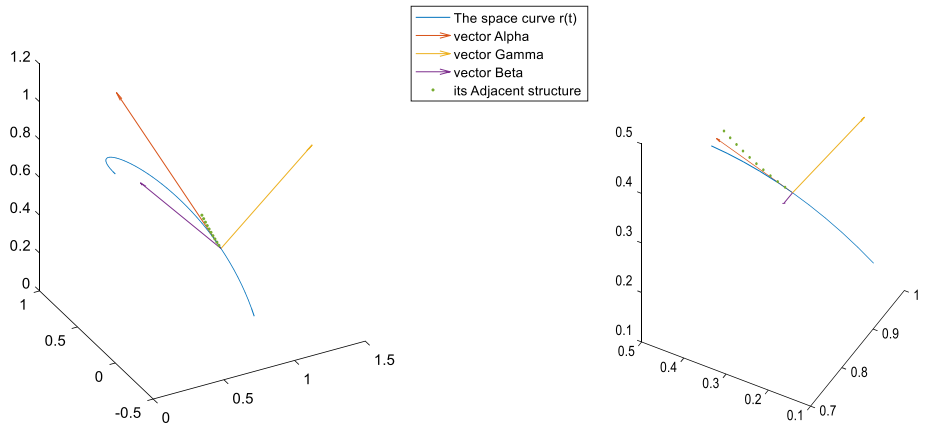

Fig. 2 The adjacent structure of the space curve at point $t_0 = \frac{\pi}{10}$

$$x = s, y = \frac{1}{2}\kappa_0 s^2, z = \frac{1}{2}\kappa_0\tau_0 s^2,$$

where s is a length parameter of the curve.

Choose an interval $\left[0, \frac{\pi}{2}\right]$ at point $t_0{=}\frac{\pi}{10}$. Combined the space coordinate (x, y, z) of the adjacent points and Frenet frame at point $t_0{=}\frac{\pi}{10}$, the adjacent structure and tangent vectors of the space curve at point $t_0{=}\frac{\pi}{10}$ are shown in the left graph of Fig. 2. The raw space curve is shown by the blue curve. In order to demonstrate the adjacent structure more clearly and intuitively, local enlarged detail is shown in the right graph of Fig. 2. The $\vec{\alpha}$ is shown by the orange vector, the $\vec{\beta}$ is shown by the purple vector, and the $\vec{\gamma}$ is shown by yellow vector. The green curve implicates an approximation of the spatial curve at point $t_0{=}\frac{\pi}{10}$. The closer to the point $t_0{=}\frac{\pi}{10}$, the better the green curve is approximated to the raw blue curve(seen in the right graph of Fig. 2).

Example 2.2 Consider the adjacent structure of a point on a circular helix. For a circular helix, it satisfies the following equation:

$$\vec{r} = \{(a + v_0\cos(\omega t))\cos t, (a + v_0\cos(\omega t))\sin t, v_0\sin(\omega t)\}. \tag{6}$$

For a circular helix, choose the parameters $a = 6, v_0 = 1, \omega = 8$. so

$$\vec{r} = \{(6 + \cos(8t))\cos t, (6 + \cos(8t))\sin t, \sin(8t)\}. \tag{7}$$

Its figure is shown in Fig. 3. By computing simply, its tangent vector is obtained as

$$\vec{r'} = \{-(6 + \cos 8t)\sin t - 8\sin 8t\cos t, (6 + \cos 8t)\cos t - 8\sin 8t\sin t, 8\cos(8t)\}.$$

Moreover,

$$\left\langle \vec{r}, \vec{r'} \right\rangle = -48\sin 8t$$

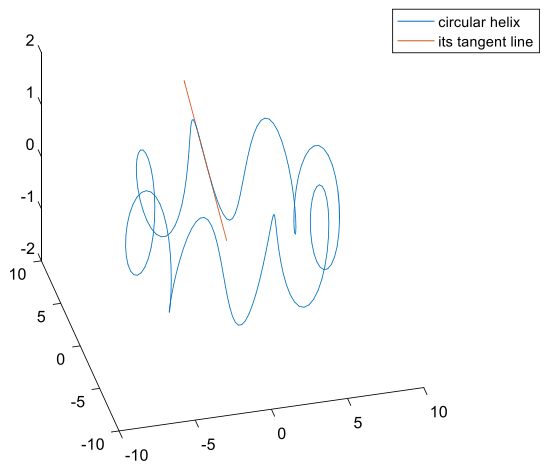

Fig. 3 A circular helix and its tangent line

It shows that the vector $\vec{r}$ is orthogonal with its tangent vector $\vec{r'}$ at some points $t = \frac{k\pi}{8}, k \in Z$, such as $t = \frac{\pi}{8}, \frac{\pi}{4}$ and so on.

Note 1 At some points, the vector $\vec{r}$ is orthogonal with its tangent vector $\vec{r'}$.The calculation at these points are relatively simple in the construction of the local tangent projection. Naturally, they are the more appropriate points for constructing the projection.

Choose $t_0{=}\frac{\pi}{2}$ and compute its tangent vector by Eq. (7). The figure of its tangent line at point $t_0{=}\frac{\pi}{2}$ is shown in Fig. 3. The Frenet frame at point $t_0{=}\frac{\pi}{2}$ can be established by Eq. (4). However, by computing the curvature κ_0 and scratch rate τ_0 at point $t_0{=}\frac{\pi}{2}$, the space coordinate (x, y, z) of the adjacent points can be denoted by

$$x = s, y = \frac{1}{2}\kappa_0 s^2, z = \frac{1}{2}\kappa_0\tau_0 s^2,$$

where s is a length parameter of the curve. The above equations show the new coordinate near the point $\vec{r}\left(\frac{\pi}{2}\right)$. It implies the approximate curve shape near the point $\vec{r}\left(\frac{\pi}{2}\right)$ of the original curve, that is determined by the curvature κ_0 and scratch rate τ_0 at point $t_0{=}\frac{\pi}{2}$. It is also the approximate for the tangent line.

Combined the space coordinate (x, y, z) of the adjacent points and Frenet frame at point $t_0{=}\frac{\pi}{2}$, the adjacent structure of the space curve at point $t_0{=}\frac{\pi}{2}$ is shown in Fig. 4. It implies an approximation of the spatial curve at point $t_0{=}\frac{\pi}{2}$.

Choose an interval $[0, 1]$ of length parameter s at point $t_0{=}\frac{\pi}{2}$, that is,$s \in [0, 1][0, 1]$. Combined the space coordinate (x, y, z) of the adjacent points and Frenet frame at point $t_0{=}\frac{\pi}{2}$, the adjacent structure and tangent vectors at point $t_0{=}\frac{\pi}{2}$ are shown in the left graph of Fig. 4. The raw space curve is shown by the blue curve. In order to demonstrate the adjacent structure more clearly and intuitively, local enlarged detail is shown in the right graph of Fig. 4. The $\vec{\alpha}$ is shown by the orange vector, the $\vec{\beta}$ is shown by the purple vector, and the $\vec{\gamma}$ is shown by yellow vector. The green dotted curve implicates an approximation of the spatial curve at point $t_0{=}\frac{\pi}{2}$. The closer to the point $t_0{=}\frac{\pi}{2}$, the better the green dotted curve is approximated to the raw blue curve (seen in the right graph of Fig. 4).

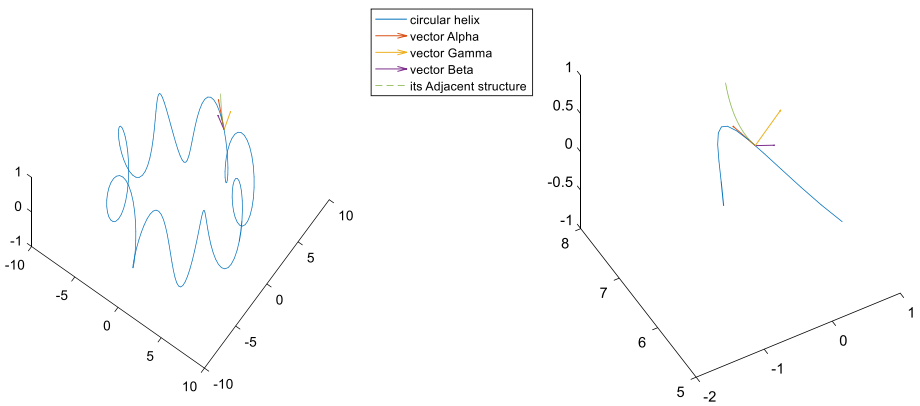

Fig. 4 The adjacent structure of the space curve at point $t_0{=}\frac{\pi}{2}$

2.2 Some Projection for a helix space curves

2.2.1 Projection from a spatial curve on the unit sphere to its tangent line

According to the theory of the vector algebra, a projection of a vector onto a axis or direction vector can be defined by their inner product. Consider the space curve on a unit sphere in Example 2.1 and its tangent vector at point t_0 can be expressed as follows:

$$\vec{r'}(t_0) = \{-\sin(2t_0), \cos(2t_0), \cos(t_0)\}.$$

So $\left|\vec{r'}(t_0)\right| = \sqrt{\cos^2 t_0 + 1}$. The unit tangent vector $\vec{\alpha}(t_0)$ at point t_0 can be computed by

$$\vec{\alpha}(t_0) = \frac{\vec{r'}(t_0)}{\left|\vec{r'}(t_0)\right|}.$$

The projection of a space curve on a unit sphere onto its tangent line can be constructed as follows:

$$P : \vec{r}(t) \to \vec{r}(t_0) + \left\langle \vec{r}(t), \vec{\alpha}(t_0) \right\rangle \vec{\alpha}(t_0). \tag{8}$$

From this projection, The distance from the projection point on the tangent line to point t_0 is the inner product $\left|\left\langle \vec{r}(t), \vec{\alpha}(t_0) \right\rangle\right|$. A number axis with the point $\vec{r}(t_0)$ as the origin is established by the tangent line of the point $\vec{r}(t_0)$ on the curve $\vec{r}(t)$. There is a neighbourhood at point t_0 such that a one-to-one correspondence is established between the real numbers $\left\langle \vec{r}(t), \vec{\alpha}(t_0) \right\rangle$ and a point on this axis. So the projection of a space curve on the unit sphere onto its tangent line can be defined as:

$$p : t \to T = \left\langle \vec{r}(t), \vec{\alpha}(t_0) \right\rangle. \tag{9}$$

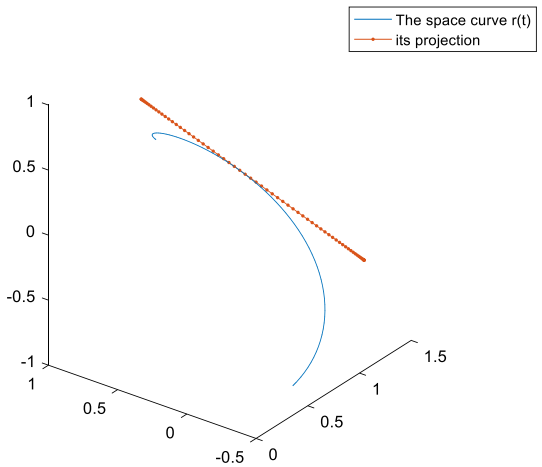

Fig. 5 Figures of the local space curve at point $t_0 = \frac{\pi}{10}$ and its projection

The local space curve at point $t_0=\frac{\pi}{10}$ is shown in Fig. 3. And its projection is also given in Fig. 5. Take the Example2.1 as an example. The local space curve at the interval $\left(-\frac{3\pi}{10}, \frac{4\pi}{10}\right)$, that is a neighborhood of point $t_0=\frac{\pi}{10}$, is shown by the blue curve in Fig. 5. This local space curve is projected onto its tangent line by the projection p at point $t_0=\frac{\pi}{10}$ in Eq. (8), which is shown as the red line in Fig. 5.

2.2.2 Length-preserving projection for a circular helix

Similar to the area-preserving projection [13], it is convenient to lift the traditional multi-resolution analysis onto a smooth curve (more detail can be seen in relative work [5, 6, 13, 22]). According to the algorithm of discretization length-preserving projection p on a smooth curve [5, 6], the discretized projection p is obtained in this section.

Consider a circular helix $\mathbb{C}$:

$$\vec{r} = \{(a + v_0 \cos(\omega t)) \cos t, (a + v_0 \cos(\omega t)) \sin t, v_0 \sin(\omega t)\}.$$

Choose the parameters $a = 6, v_0 = 1, \omega = 8$. So

$$\vec{r} = \{(6 + \cos(8t)) \cos t, (6 + \cos(8t)) \sin t, \sin(8t)\}.$$

By calculating, we have

$$dL = \sqrt{64 + (6 + \cos 8t)^2}dt. \tag{10}$$

According to the Euler discretization method: For a finite interval $[T_0, T_1]$, $T_0 = t_0 < t_1 < \cdots < t_n = T_1$, then, then

$$dL = \sqrt{64 + (6 + \cos 8t)^2}dt \Leftrightarrow \sqrt{64 + (6 + \cos 8t_{i-1})^2}\Delta t_i = \Delta L_i$$

where $\Delta t_i = t_i - t_{i-1}, \Delta L_i = L_i - L_{i-1}$.

The discretization length-preserving projection p can be denoted as follows:

$$p : t_i \to L_i = L_{i-1} + \sqrt{64 + (6 + \cos 8t_{i-1})^2}(t_i - t_{i-1})$$

where $(x_0, y_0, z_0) \to L_0 = 0$. And its inverse p^{-1} is

$$p^{-1} : L_i \to t_i = t_{i-1} + \frac{1}{\sqrt{64 + (6 + \cos 8t_{i-1})^2}}(L_i - L_{i-1}), \tag{11}$$

$$(x(t_i), y(t_i), z(t_i)) = \{(6 + \cos(8t_i)) \cos t_i, (6 + \cos(8t_i)) \sin t_i, \sin(8t_i)\},$$

where $L_0 \to t_0, (x(t_0), y(t_0), z(t_0))$ can be obtained.

For example, Fig. 6 shows that a circular helix with length 12 is projected onto a straight line with the same length by the discretized length-preserving projection p. In the other word, by the discretized inverse projection p^{-1}, every point on the straight line with length 12 can be projected to the corresponding point on the circular helix.

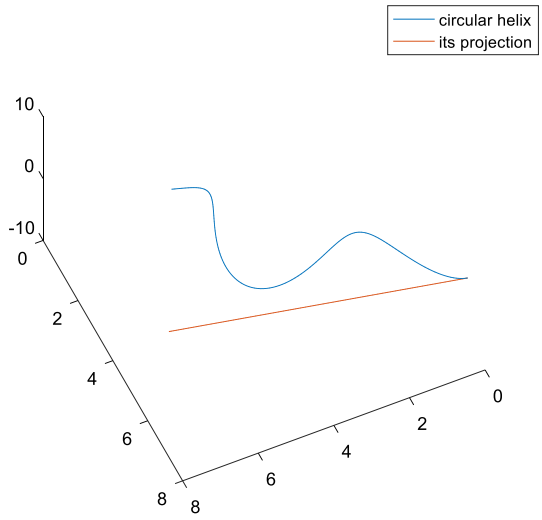

Fig. 6 Projecting a circular helix to a straight line by length-preserving projection p

3 The local continuous wavelet transform on a space curve

Assume that $\wp = L^2(C, d\mu)$ be a Hilbert space of the square integrable function on a space curve C, with a suitable measure $d\mu$ and the scaling product $< \cdot, \cdot >_{\wp}$. The symbol $T_{\xi}(C)$ denote the tangent space at $\xi \in C$. In order to discuss the local wavelet transform on a space curve C, a compactly supported square integrable function $\psi^{(\xi)} \in \wp$ should be constructed as a mother wavelet in the neighborhood $B_{(\xi)}$, $\xi \in C$. The size of $B_{(\xi)}$ depends on the property of the local geometry of C. Moreover, a suitable local dilation operator need to be defined on a space curve C. In order to establish wavelet basis on a space curve C by dilating and translating the mother wavelet, an effective method is That the points in the neighborhood $B_{(\xi)}$ is projected onto the tangent line at and then the dilated and translated points are pulled back onto the space curve. In the follows, consider a space curve on a unit ball as an example.

According to the discussion in Sect. 2.1, the projection from a space curve on a unit sphere onto its tangent line can be constructed as follows:

$$p_{t_0} : t \to T = \left\langle \vec{r}(t), \vec{\alpha}(t_0) \right\rangle \tag{12}$$

So $p_{t_0}(t_0) = T_0 = 0$. According to the equations of a spatial curve in Sect. 2, the inner product $\left\langle \vec{r}(t), \vec{\alpha}(t_0) \right\rangle$ can be computed. It is easy to see that p_{t_0} is continuous and there exists an interval I containing t_0 such that p_{t_0} is a diffeomorphism.

In Ref. [2], the local dilation of coordinates is defined as

$$d_a : t \mapsto t_a = p_{t_0}^{-1} \cdot a \cdot p_{t_0},\ a > 0$$

And the maximum local dilation at point t_0 is $a_{\max} = \sup_{t \in I} p_{t_0}$, where a is a positive real number dilation factor in Sect. 3. So, $p_{t_0}(t_a) = a \cdot p_{t_0}(t)$.

Similar to Ref. [2], a dilation operator is constructed for acting on functions with a support in $B_{(\xi_0)}$. A subspace of $\wp$ is denoted by $\wp(B_{(\xi_0)})$. Given a wavelet function $\psi^{(\xi_0)} \in \wp(B_{(\xi_0)})$, the dilation operator of $\psi^{(\xi_0)}$ is defined as follows:

$$D_{\xi_0}(a) : \psi^{(\xi_0)}(t) \mapsto \lambda^{\frac{1}{2}}(a,t)\psi^{(\xi_0)}\left(t_{a^{-1}}\right) \tag{13}$$

where $\xi_0 = \overrightarrow{r}(t_0)$ and $\lambda(a,t)$ is the corresponding Radon-Nikodym derivative defined as

$$\lambda(a,t) = \frac{d\mu(t_{a^{-1}})}{d\mu(t)} \tag{14}$$

which is related to the possible change of the measure μ under the dilation. According to the differential method for an implicit function, Radon-Nikodym derivative $\lambda(a,t)$ can be obtained from the equation $p_{t_0}(t_a) = a \cdot p_{t_0}(t)$, that is,

$p'_{t_0}(t_a)d\mu(t_a) = a \cdot p'_{t_0}(t)d\mu(t)$.

So

$$\lambda(a,t) = \frac{d\mu(t_{a^{-1}})}{d\mu(t)} = \frac{a^{-1}p'_{t_0}(t)}{p'_{t_0}(t_{a^{-1}})}. \tag{15}$$

If there exists a $t^*_{a^{-1}}$ such that $p_{t_0}(t^*_{a^{-1}}) = a^{-1} \cdot p_{t_0}(t) - p(b)$, where $\overrightarrow{r}(b) \in C$,

$$\lambda(a,t) = \frac{d\mu(t^*_{a^{-1}})}{d\mu(t)} = \frac{d\mu(t_{a^{-1}})}{d\mu(t)} = \frac{a^{-1}p'_{t_0}(t)}{p'_{t_0}(t_{a^{-1}})}. \tag{16}$$

If $\psi^{(\xi_0)}$ is a bounded function with compactly supported in $[t_0 - \varepsilon, t_0 + \varepsilon] \subset I$, the shorter notation $\psi_a^{(\xi_0)}$ can be used for denoting the expression $D_\xi(a)\psi^{(\xi_0)}(t)$, that is

$$\psi_a^{(\xi_0)} := \lambda^{\frac{1}{2}}(a,t)\psi^{(\xi_0)}\left(t_{a^{-1}}\right),$$

and the maximum local dilation applicable to the wavelet $\psi_a^{(\xi_0)}$ is $a_{\max} = a_{\psi^{(\xi_0)}}$.

Moreover, the translation of a function $\psi^{(\xi_0)}$ can be defined at point ξ_0 by

$$T_b\psi^{(\xi_0)}(t) = \psi^{(\xi_0)} \circ p^{-1}(p(t) - p(b)),$$

where $\overrightarrow{r}(b) \in C$. Acting the dilation operator and translation on the function $\psi^{(\xi_0)}(t)$ yields a simple expression:

$$\psi_{a,b}^{(\xi_0)}(t) = \lambda^{1/2}(a,t)\psi^{(\xi_0)} \circ p^{-1}(a^{-1}p(t) - p(b)). \tag{17}$$

If a signal $f \in \wp(B_{(\xi_0)})$, the continuous wavelet transform between the signal $f(t)$ and dilated wavelet can be rewritten as the following form:

$$\begin{aligned} W_{\psi_{a,b}^{(\xi_0)}} f &= \left\langle f, \psi_{a,b}^{(\xi_0)} \right\rangle_{\wp} = \int_C f(t)\overline{\psi_{a,b}^{(\xi_0)}}dt \\ &= \int_C \lambda^{\frac{1}{2}}(a,t)\overline{\psi^{(\xi_0)} \circ p^{-1}(a^{-1}p(t) - p(b))}f(t)dt. \end{aligned} \tag{18}$$

Definition 3.1 Assume that $\psi^{(\xi_0)} \in \wp(B(\xi_0))$, which satisfies

$$0 < C_\psi = \int_0^{a_\psi(\phi)} \frac{\left\|\hat{\psi}(\omega_a)\right\|^2}{a^2}da < \infty. \tag{19}$$

Then $\psi^{(\xi_0)}$ is a local mother wavelet on a space curve on a unit ball, and Eq. (19) is called the admissibility condition.

Theorem 3.1 (Reconstruction formula). *Assume that* $\psi^{(\xi_0)} \in \wp(B(\xi_0))$, *a function* $f \in \wp(B_{(\xi_0)})$, *the local wavelet transform of* f *at a point* ξ_0 *is* $W_{\psi_{a,b}^{(\xi_0)}} f(a,b)$, *then for every* $f \in \wp(B_{(\xi_0)})$, *there is*

$$C_{\psi^{(\xi_0)}} f(t) = \int_C \int_0^{a_{\psi^{(\xi_0)}}} W_{\psi_{a,b}^{(\xi_0)}} f(a,b) \psi_a^{(\xi_0)}(t) \frac{da}{a^2} dt_0 \tag{20}$$

The result of Theorem 3.1 *is similar to the conclusions in the literature* [12, 15, 21].

4 Lifting discrete wavelet transform on a helix space curve $\mathbb{C}$ via length-preserving projection

In this section, discrete wavelet transform is lifted onto a helix space curve by length-preserving projection. Some conclusions are similar to the results in [1, 5, 13, 14].

Assume that a helix space curve $\mathbb{C}$ satisfies parameter equation in Eq. (3):

$$\xi = (x(t), y(t), z(t)) = \{(a + v_0 \cos(\omega t)) f(t), (a + v_0 \cos(\omega t)) g(t), v_0 \sin(\omega t)\}, t \in R.$$

A length-preserving projection $p : \xi \to X$ is constructed in Sect. 2.2.2. It is obviously bijective and its inverse is $p^{-1} : X \to \xi$. The length-preserving projection p means that the length element $dL(\xi)$ on a helix space curve is equal to the length element dX on a line.

According to length-preserving projection p, for arbitrary functions $\tilde{f}, \tilde{g} \in L^2(\mathbb{C})$, we have

$$< \tilde{f}, \tilde{g} >_{L^2(\mathbb{C})} = < \tilde{f} \circ p^{-1}, \tilde{g} \circ p^{-1} >_{L^2(R)} . \tag{21}$$

Similarly, If $f, g \in L^2(R)$,

$$< f, g >_{L^2(R)} = < f \circ p, g \circ p >_{L^2(\mathbb{C})} . \tag{22}$$

In order to establish the multi-resolution analysis of $L^2(\mathbb{C})$, the multi-resolution analysis [23–29] of $L^2(R)$ and a useful Lemma are rewritten as follows. For an increasing sequence of closed subspace V_j, where $V_j = clos_{L^2(R)} < \phi_{j,k} = 2^{j/2}\phi(2^j t - k) : k \in Z >$, $\phi_{j,k} = 2^{j/2}\phi(2^j t - k)$, $\phi \in L^2(R)$, it satisfies the following conditions:

(1) $V_j \subset V_{j+1}, \forall j \in Z$;
(2) $\bigcap_{j \in Z} V_j = \{0\}$, $\overline{\bigcup_{j \in Z} V_j} = L^2(R)$;
(3) $f(t) \in V_j \Rightarrow f(2t) \in V_{j+1}$;
(4) there exists a function $\phi(t) \in L^2(R)$ the set $\{\phi(t-k), k \in Z\}$ is a orthogonal basis of V_0.

Lemma 4.1 ([5, 6, 13, 22]) *Assume that J be a countable set and* $\{f_k\}_{k\in J} \in L^2(R)$. *For each* $k \in J$, *we define* $\{\tilde{f}_k\}_{k\in J} \in L^2(\mathbb{C})$ *as* $\tilde{f}_k = f_k \circ p$. *Then we have*:

(1) *If* $\{f_k\}_{k\in J}$ *is an orthogonal basis of* $L^2(R)$, *then* $\{\tilde{f}_k\}_{k\in J}$ *is also an orthogonal basis of* $L^2(\mathbb{C})$.
(2) *If* $\{f_k\}_{k\in J}$ *is a Reisz basis of* $L^2(R)$ *with Riesz constants A and B, then* $\{\tilde{f}_k\}_{k\in J}$ *is a Reisz basis of* $L^2(\mathbb{C})$ *with the same Riesz constants.*
(3) *If* $\{f_k\}_{k\in J}$ *is a frame of* $L^2(R)$ *with frame bounds A and B, then* $\{\tilde{f}_k\}_{k\in J}$ *is a Reisz basis of* $L^2(\mathbb{C})$ *with the same frame bounds.*

Based on Lemma 4.1, Eqs. (21) and (22), we have the following definition.

Definition 4.1 ([1, 5, 13, 14]) If a sequence of subspaces v_j satisfy the following properties

(1) $v_j \subset v_{j+1}, \forall j \in Z$;
(2) $\bigcap_{j\in Z} v_j = \{0\}, \overline{\bigcup_{j\in Z} v_j} = L^2(\mathbb{C})$;
(3) $f^{\mathbb{C}} \in v_j \Rightarrow D_2 f^{\mathbb{C}} \in v_{j+1}$, where D_2 is defined in Eq. (24);
(4) the set $\{\phi^{\mathbb{C}}_{0,k}, k \in Z\}$ is an orthogonal basis of v_0, where $v_j = clos_{L^2(R)} < \phi^{\mathbb{C}}_{j,k} : k \in Z >$,

$\phi^{\mathbb{C}}_{j,k} = \phi_{j,k} \circ p$, an orthogonal multi-resolution analysis of $L^2(\mathbb{C})$ is generated by the induced subspaces v_j.

Note 2 From property (1) to property (4), they are consistent monotony, asymptotic completeness, scaling regularity, existence of orthogonal bases, respectively. These properties are lifted onto a helix space curve $\mathbb{C}$.

For every $j \in Z$, assume that w_j denotes an orthogonal complement of coarse space v_j into v_{j+1} such that $v_{j+1} = v_j \oplus w_j$. The w_j is called the wavelet subspace into v_{j+1}. If there is a wavelet function ψ, the function $\psi^{\mathbb{C}}$ on a helix space can be induced by $\psi^{\mathbb{C}} = \psi \circ p$. It is easy to see that for each $j \in Z$, $\{\psi^{\mathbb{C}}_{j,k}, k \in Z\}$ is an orthogonal basis of w_j and so $\{\psi^{\mathbb{C}}_{j,k}, j \in Z, k \in Z\}$ is an orthogonal basis of $\overline{\oplus_{j\in Z} w_j} = L^2(\mathbb{C})$. Thus $\phi^{\mathbb{C}}$ is called the scaling function on a helix space curve $\mathbb{C}$, and $\psi^{\mathbb{C}}$ is called the corresponding wavelet on a helix space curve $\mathbb{C}$.

The translation operator and dilation operator in the space $L^2(\mathbb{C})$ can be defined as follows:

$$(1)\ \text{Translation operator}: T_b\phi^{\mathbb{C}}(\xi) = \left(\phi^{\mathbb{C}} \circ p^{-1}\right)(p(\xi) - b), b \in R; \tag{23}$$

$$(2)\ \text{Dilation operator}: D_a\phi^{\mathbb{C}}(\xi) = \left(\phi^{\mathbb{C}} \circ p^{-1}\right)(a \cdot p(\xi)), a > 0; \tag{24}$$

where $\phi^{\mathbb{C}} \in L^2(\mathbb{C})$, and combining two operators, a unitary operator $U(b, a) = D_a T_b$ can be written as:

$$\left[U(b,a)\phi^{\mathbb{C}}\right](\xi) = \left(\phi^{\mathbb{C}} \circ p^{-1}\right)(a \cdot p(\xi) - b).$$

According to the induced multi-resolution analysis of $L^2(\mathbb{C})$, for a scaling function $\phi^{\mathbb{C}} \in L^2(\mathbb{C})$, the two-scale equation can be deduced as follows:

$$\phi^{\mathbb{C}}(\xi) = \sum_{k\in Z} h_k^{\mathbb{C}} \left[U(k,2)\phi^{\mathbb{C}}\right](\xi) = \sum_{k\in Z} h_k^{\mathbb{C}} \left(\phi^{\mathbb{C}} \circ p^{-1}\right)(2 \cdot p(\xi) - k), \tag{25}$$

where a sequence $\{h_k^{\mathbb{C}}\}$ is called the two-scale sequence of $\phi^{\mathbb{C}}(\eta)$. Based on the length-preserving projection p, the associated function $\phi = \phi^{\mathbb{C}} \circ p^{-1}$ satisfies the two-scale equation:

$$\phi(x) = \sum_{k\in Z} h_k \phi(2x - k),$$

where a sequence $\{h_k\}$ is the two-scale sequence of ϕ. the sequence $\{h_k^{\mathbb{C}}\}$ has the following conclusion.

Theorem 4.1 *Assume that p is a length-preserving projection from a helix space curve $\mathbb{C}$ to a subset of real axis X. If $\phi^{\mathbb{C}}$ is the scaling function in $L^2(\mathbb{C})$, which is induced from $\phi \in L^2(R)$ by p, then the sequences $\{h_k\}$ and $\{h_k^{\mathbb{C}}\}$ satisfy $h_k^{\mathbb{C}} = h_k$, where the sequences $\{h_k\}$ is the two-scale sequence of the scaling function φ.*

Similar to the results in Ref. [1, 5, 6], the Fourier transform of $\phi^{\mathbb{C}}$ in (24) is obtained as follows:

$$\hat{\phi}^{\mathbb{C}}(\varpi) = H^{\mathbb{C}}\left(\frac{p(\varpi)}{2}\right)\widehat{\phi^{\mathbb{C}} \circ p^{-1}}\left(\frac{p(\varpi)}{2}\right), \tag{26}$$

where $H^{\mathbb{C}}\left(\frac{p(\varpi)}{2}\right) = \frac{1}{2}\sum_{k\in Z} h_k^{\mathbb{C}} e^{-\frac{ip(\varpi)\cdot k}{2}}$ is called the two-scale symbol and $p(\varpi) = \omega, \varpi \in \mathbb{C}$.

According to the results of orthogonality in Refs. [1, 5, 6, 23, 24], the similar conclusion can be obtained in the following theorem.

Definition 4.2 The scaling function $\phi^{\mathbb{C}}(\eta)$ in $L^2(\mathbb{C})$ is orthonormal, if it satisfies the following equation:

$$\left\langle \phi^{\mathbb{C}}(\eta), \left(T_k\phi^{\mathbb{C}}\right)(\eta)\right\rangle = \delta_{0,k}. \tag{27}$$

Theorem 4.2 *If the scaling function $\phi^{\mathbb{C}}(\eta)$ in $L^2(\mathbb{C})$ is orthonormal, the following statements are equivalent*:

(1) $\left\{\left(T_k\phi^{\mathbb{C}}\right)(\eta) | k \in Z\right\}$ *is orthonormal, that is* $\left\langle \phi^{\mathbb{C}}(\eta), \left(T_k\phi^{\mathbb{C}}\right)(\eta)\right\rangle = \delta_{0,k}$;

(2) $\sum_{k\in Z} \left|\widehat{\phi^{\mathbb{C}} \circ p^{-1}}(\omega + 2k\pi)\right|^2 = 1$, *a.e.* $\omega \in R$;

(3) $\sum_{k\in Z} h_k^{\mathbb{C}} \overline{h_{k+2n}^{\mathbb{C}}} = 2\delta_{0,n}$;

(4) $H^{\mathbb{C}}\left(\frac{p(\varpi)}{2}\right)\overline{H^{\mathbb{C}}\left(\frac{p(\varpi)}{2}\right)} + H^{\mathbb{C}}\left(\frac{p(\varpi)}{2}+\pi\right)\overline{H^{\mathbb{C}}\left(\frac{p(\varpi)}{2}+\pi\right)} = 1$

Proof (1) ⇔ (2)

Since $\left\{\left(T_k\phi^{\mathbb{C}}\right)(\eta)|k\in Z\right\}$ is orthonormal, that is $\left\langle\phi^{\mathbb{C}}(\eta),\left(T_k\phi^{\mathbb{C}}\right)(\eta)\right\rangle = \delta_{0,k}, k\in Z.$

According to Eq. (29),

$$\delta_{0,k} = \left\langle\phi^{\mathbb{C}}(\eta),\left(T_k\phi^{\mathbb{C}}\right)(\eta)\right\rangle_{L^2(\mathbb{C})} = \left\langle\phi^{\mathbb{C}}\circ p^{-1}(t),\phi^{\mathbb{C}}\circ p^{-1}(t-k)\right\rangle_{L^2(R)}, p(\eta)=t.$$

Then $\left\{\phi^{\mathbb{C}}\circ p^{-1}(t-k)|k\in Z\right\}$ is also orthonormal. So

$$\left\langle\phi^{\mathbb{C}}\circ p^{-1}(t),\phi^{\mathbb{C}}\circ p^{-1}(t-k)\right\rangle_{L^2(R)} = \delta_{0,k} \text{ is equal to } \sum_{k\in Z}\left|\widehat{\phi^{\mathbb{C}}\circ p^{-1}}(\omega+2k\pi)\right|^2 = 1.$$

(1) ⇔ (3),

$$\begin{aligned}
\delta_{0,k} &= \left\langle\phi^{\mathbb{C}}(\eta),\left(T_k\phi^{\mathbb{C}}\right)(\eta)\right\rangle = \int_C \phi^{\mathbb{C}}(\eta)\overline{\left(T_k\phi^{\mathbb{C}}\right)(\eta)}dL(\eta)\\
&= \int_C \phi^{\mathbb{C}}(\eta)\overline{\left(\phi^{\mathbb{C}}\circ p^{-1}\right)(p(\eta)-k)}dL(\eta)\\
&= \int_R \phi^{\mathbb{C}}(p^{-1}(X))\overline{\left(\phi^{\mathbb{C}}\circ p^{-1}\right)(p(p^{-1}(X))-k)}dX\\
&= \int_R \phi(X)\overline{\phi(X-k)}dX\\
&= \frac{1}{2}\sum_{l\in Z} h_l\overline{h_{k+2n}} = \frac{1}{2}\sum_{l\in Z} h_l^{\mathbb{C}}\overline{h_{k+2n}^{\mathbb{C}}}.
\end{aligned}$$

(2) ⇔ (4),

$$\begin{aligned}
1 &= \sum_{k\in Z}\left|\widehat{\phi^{\mathbb{C}}\circ p^{-1}}(p(\varpi)+2k\pi)\right|^2 = \sum_{k\in Z}\left|H^{\mathbb{C}}\left(\frac{p(\varpi)}{2}+k\pi\right)\widehat{\phi^{\mathbb{C}}\circ p^{-1}}\left(\frac{p(\varpi)}{2}+k\pi\right)\right|^2\\
&= \sum_{k\in Z}\left|H^{\mathbb{C}}\left(\frac{p(\varpi)}{2}+2k\pi\right)\widehat{\phi^{\mathbb{C}}\circ p^{-1}}\left(\frac{p(\varpi)}{2}+2k\pi\right)\right|^2\\
&\quad + \sum_{k\in Z}\left|H^{\mathbb{C}}\left(\frac{p(\varpi)}{2}+(2k+1)\pi\right)\widehat{\phi^{\mathbb{C}}\circ p^{-1}}\left(\frac{p(\varpi)}{2}+(2k+1)\pi\right)\right|^2\\
&= \left|H^{\mathbb{C}}\left(\frac{p(\varpi)}{2}\right)\right|^2 + \left|H^{\mathbb{C}}\left(\frac{p(\varpi)}{2}+\pi\right)\right|^2.
\end{aligned}$$

The theorem is obtained.

According to the multi-resolution analysis, for the wavelet function $\psi^{\mathbb{C}}(\eta)$ corresponding to the scaling function $\phi^{\mathbb{C}}(\eta)$, it satisfies the following two-scale equation:

$$\psi^{\mathbb{C}}(\eta) = \sum_{k\in Z} g_k^{\mathbb{C}}\left[U(k,2)\phi^{\mathbb{C}}\right](\eta) = \sum_{k\in Z} g_k^{\mathbb{C}}\left(\phi^{\mathbb{C}}\circ p^{-1}\right)(2\cdot p(\eta)-k) \tag{28}$$

where the sequence $\{g_k^{\mathbb{C}}\}$ is called the two-scale sequence of $\psi^{\mathbb{C}}(\eta)$. Based on the length-preserving projection p, the sequence $\{g_k^{\mathbb{C}}\}$ has the following conclusion.

Theorem 4.3 *Assume that p is a length-preserving projection from a helix space curve $\mathbb{C}$ to a subset of real axis X. If $\phi^{\mathbb{C}}$ is the scaling function in $L^2(\mathbb{C})$, which is induced from $\phi \in L^2(R)$, and $\psi^{\mathbb{C}} \in L^2(\mathbb{C})$ is the wavelet function induced from $\psi \in L^2(R)$, then the sequences $\{g_k\}$ and $\{g_k^{\mathbb{C}}\}$ satisfy $g_k^{\mathbb{C}} = g_k$, where the sequences $\{g_k\}$ is the two-scale sequence of the wavelet function.*

Similar to the results in Ref. [1, 5, 6], the Fourier transform of $\psi^{\mathbb{C}}$ in (26) is obtained as follows:

$$\psi^{\mathbb{C}}(\varpi) = G^{C}\left(\frac{p(\varpi)}{2}\right)\phi^{\mathbb{C}} \overset{\wedge}{\circ} p^{-1}\left(\frac{p(\varpi)}{2}\right) \tag{29}$$

where $G^{\mathbb{C}}\left(\frac{p(\varpi)}{2}\right) = \frac{1}{2}\sum_{k\in Z} g_k^{\mathbb{C}} e^{-\frac{ip(\varpi)\cdot k}{2}}$ is called to be the two-scale symbol of $\psi^{\mathbb{C}}(\eta)$.

Definition 4.3 The wavelet $\psi^{\mathbb{C}}(\eta)$ corresponding to the scaling function $\phi^{\mathbb{C}}(\eta)$ in $L^2(\mathbb{C})$ is orthonormal. If the following equations hold:

$$\begin{cases} \left\langle \phi^{\mathbb{C}}(\eta), \left(T_k\psi^{\mathbb{C}}\right)(\eta)\right\rangle_{L^2(\mathbb{C})} = 0, \\ \left\langle \psi^{\mathbb{C}}(\eta), \left(T_k\psi^{\mathbb{C}}\right)(\eta)\right\rangle_{L^2(\mathbb{C})} = \delta_{0,k}. \end{cases} \tag{30}$$

Theorem 4.4 *Assume that p is a length-preserving projection from a helix space curve $\mathbb{C}$ to a subset of real axis X. The wavelet $\psi^{\mathbb{C}}(\eta)$ corresponding to the scaling function $\phi^{\mathbb{C}}(\eta)$ in $L^2(\mathbb{C})$ is orthonormal, then the following statements are equivalent*:

(1) *The wavelet $\psi^{\mathbb{C}}(\eta)$ is orthonormal, that is, Eq. (34) holds.*
(2) *If the wavelet $\psi^{\mathbb{C}}(\eta)$ is orthonormal, the sequence $\{g_k^{\mathbb{C}}\}$ satisfies*

$$\begin{cases} \sum\limits_{k\in Z} h_k^{\mathbb{C}}\overline{g_{k+2n}^{\mathbb{C}}} = 0, \\ \sum\limits_{k\in Z} g_k^{\mathbb{C}}\overline{g_{k+2n}^{\mathbb{C}}} = 2\delta_{0,n}. \end{cases} \tag{31}$$

(3) *If the wavelet $\psi^{\mathbb{C}}(\eta)$ is orthonormal, the two-scale symbol $G^{\mathbb{C}}\left(\frac{p(\varpi)}{2}\right)$ satisfies*

$$\begin{cases} H^{\mathbb{C}}\left(\frac{p(\varpi)}{2}\right)\overline{G^{\mathbb{C}}\left(\frac{p(\varpi)}{2}\right)} + H^{\mathbb{C}}\left(\frac{p(\varpi)}{2}+\pi\right)\overline{G^{\mathbb{C}}\left(\frac{p(\varpi)}{2}+\pi\right)} = 0, \\ G^{\mathbb{C}}\left(\frac{p(\varpi)}{2}\right)\overline{G^{\mathbb{C}}\left(\frac{p(\varpi)}{2}\right)} + G^{\mathbb{C}}\left(\frac{p(\varpi)}{2}+\pi\right)\overline{G^{\mathbb{C}}\left(\frac{p(\varpi)}{2}+\pi\right)} = 1. \end{cases} \tag{32}$$

Proof (1) $\Leftrightarrow$ (2) According to Theorems 4.1 and 4.4 and Eq. (34),

$$
\begin{aligned}
0 &= \left\langle \phi^{\mathbb{C}}(\eta), \left(T_k \psi^{\mathbb{C}}\right)(\eta) \right\rangle = \int_C \phi^{\mathbb{C}}(\eta) \overline{\left(T_k \psi^{\mathbb{C}}\right)(\eta)} dL(\eta) \\
&= \int_C \phi^{\mathbb{C}}(\eta) \overline{\left(\psi^{\mathbb{C}} \circ p^{-1}\right)(p(\eta) - k)} dL(\eta) \\
&= \int_R \phi^{\mathbb{C}}(p^{-1}(X)) \overline{\left(\psi^{\mathbb{C}} \circ p^{-1}\right)(p(p^{-1}(X)) - k)} dX \\
&= \int_R \phi(X) \overline{\psi(X-k)} dX \\
&= \frac{1}{2} \sum_{l \in Z} h_l \overline{g_{l+2k}} = \frac{1}{2} \sum_{l \in Z} h_l^{\mathbb{C}} \overline{g_{l+2k}^{\mathbb{C}}}.
\end{aligned}
$$

Similarly, $\sum_{k \in Z} g_k^{\mathbb{C}} \overline{g_{k+2n}^{\mathbb{C}}} = 2\delta_{0,n}$.

(2) $\Leftrightarrow$ (3)

Let a function $\phi = \phi^{\mathbb{C}} \circ p^{-1}$ be induced by $\phi^{\mathbb{C}}(\eta)$ and the wavelet function $\psi = \psi^{\mathbb{C}} \circ p^{-1}$ be induced by $\psi^{\mathbb{C}}(\eta)$. According to Theorems 4.1 and 4.4,

$$
\begin{aligned}
0 &= H\left(\frac{\omega}{2}\right) \overline{G\left(\frac{\omega}{2}\right)} + H\left(\frac{\omega}{2} + \pi\right) \overline{G\left(\frac{\omega}{2} + \pi\right)} \\
&= \frac{1}{2} \sum_{k \in Z} h_k e^{-ik\frac{\omega}{2}} \overline{\left(\frac{1}{2} \sum_{k \in Z} g_k e^{-ik\frac{\omega}{2}}\right)} + \frac{1}{2} \sum_{k \in Z} h_k e^{-ik\left(\frac{\omega}{2} + \pi\right)} \overline{\left(\frac{1}{2} \sum_{k \in Z} g_k e^{-ik\left(\frac{\omega}{2} + \pi\right)}\right)} \\
&= \frac{1}{2} \sum_{k \in Z} h_k^{\mathbb{C}} e^{-ik\frac{p(\varpi)}{2}} \overline{\left(\frac{1}{2} \sum_{k \in Z} g_k^{\mathbb{C}} e^{-ik\frac{p(\varpi)}{2}}\right)} + \frac{1}{2} \sum_{k \in Z} h_k^{\mathbb{C}} e^{-ik\left(\frac{p(\varpi)}{2} + \pi\right)} \overline{\left(\frac{1}{2} \sum_{k \in Z} g_k^{\mathbb{C}} e^{-ik\left(\frac{p(\varpi)}{2} + \pi\right)}\right)} \\
&= H^{\mathbb{C}}\left(\frac{p(\varpi)}{2}\right) \overline{G^{\mathbb{C}}\left(\frac{p(\varpi)}{2}\right)} + H^{\mathbb{C}}\left(\frac{p(\varpi)}{2} + \pi\right) \overline{G^{\mathbb{C}}\left(\frac{p(\varpi)}{2} + \pi\right)}.
\end{aligned}
$$

Analogously,

$$
G^{\mathbb{C}}\left(\frac{p(\varpi)}{2}\right) \overline{G^{\mathbb{C}}\left(\frac{p(\varpi)}{2}\right)} + G^{\mathbb{C}}\left(\frac{p(\varpi)}{2} + \pi\right) \overline{G^{\mathbb{C}}\left(\frac{p(\varpi)}{2} + \pi\right)} = 1.
$$

If a signal function $f^{\mathbb{C}}$ is square integrable on a helix space curve, that is $f^{\mathbb{C}} \in L^2(\mathbb{C})$, and the projection operators $\mathrm{P}_j^{\mathbb{C}}$ and T_j^{C}, $\mathrm{P}_j^{\mathbb{C}} f^{\mathbb{C}} \in v_j$, $\mathrm{T}_j^{\mathbb{C}} f^{\mathbb{C}} \in w_j$, then

$$
\mathrm{P}_j^{\mathbb{C}} f^{\mathbb{C}} = \sum_{k \in Z} c_{j,k}^{\mathbb{C}} \phi_{j,k}^{\mathbb{C}}, \ \mathrm{T}_j^{\mathbb{C}} f^{\mathbb{C}} = \sum_{k \in Z} d_{j,k}^{\mathbb{C}} \psi_{j,k}^{\mathbb{C}}.
$$

According to $v_{j+1} = v_j \oplus w_j$, the coefficients $c_{j,k}^{\mathbb{C}}$ and $d_{j,k}^{\mathbb{C}}$ can be computed by the length-preserving projection, Definitions 4.1 and 4.2. So the decomposition algorithm is given as follows:

$$
\begin{cases}
c_{j,k}^{\mathbb{C}} = \frac{\sqrt{2}}{2} \sum\limits_{k \in Z} c_{j+1,k}^{\mathbb{C}} \overline{h}_{k-2k'}^{\mathbb{C}} \\
d_{j,k}^{\mathbb{C}} = \frac{\sqrt{2}}{2} \sum\limits_{k \in Z} c_{j+1,k}^{\mathbb{C}} \overline{g}_{k-2k'}^{\mathbb{C}}
\end{cases}. \tag{33}
$$

The formula is similar to the traditional decomposition formula by the length-preserving projection. Moreover, the reconstruction formula can also be obtained as follows:

$$c^{\mathbb{C}}_{j+1,k} = \frac{\sqrt{2}}{2}\left(\sum_{k'\in Z} c^{\mathbb{C}}_{j,k'} h^{\mathbb{C}}_{k-2k'} + \sum_{k\in Z} d^{\mathbb{C}}_{j,k'} g^{\mathbb{C}}_{k-2k'}\right). \tag{34}$$

It is also similar to the traditional reconstruction formula by the length-preserving projection.

5 Numerical examples

In this section, two numerical examples are given for our discussion. Example 5.1 is given for discussing the applications of local continuous wavelet transform and its reconstruction formula on a space curve. Based on the length-preserving projection, discrete wavelet transform on a helix space curve is illustrated in Example 5.2.

Example 5.1 Consider a space curve on the unit sphere, and its parameter equation is given as follows:

$$\vec{r} = \{\cos(t)\cos t, \cos(t)\sin t, \sin(t)\},$$

where $t \in [-1, 1]$. By choosing the Morlet wavelet, an local Morlet wavelet at point $t = 0$ can be lifted onto the space curve by the projection of a space curve $\vec{r}(t)$ on a unit sphere in Sect. 2.2, where the Morlet [16] wavelet is

$$\psi(t) = Ce^{-\frac{t^2}{2}}\cos 5t$$

and C is the normalized constant in the reconstruction. The figures are shown in the Fig. 7. The first row and first column graph of Fig. 7 shows the graph of the Morlet wavelet, and the second row and first column graph of Fig. 7 gives the graph of the local

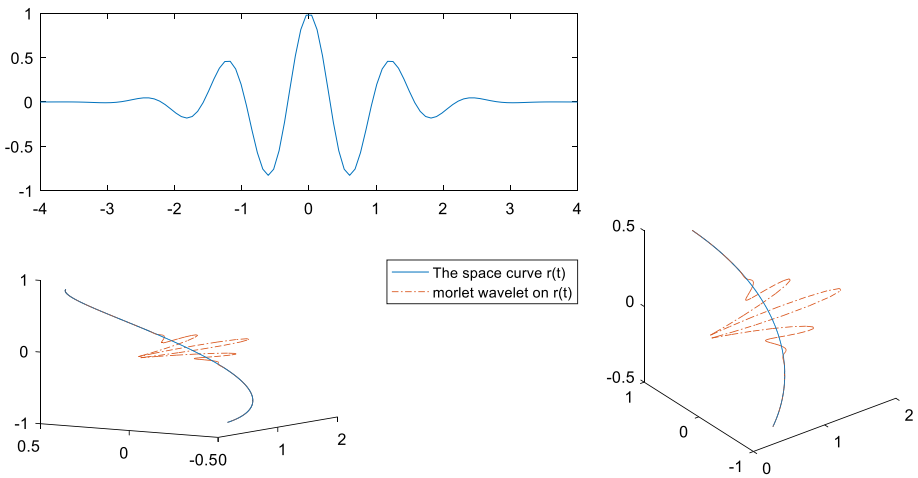

Fig. 7 Morlet wavelet and local Morlet wavelet at point $t = 0$

Morlet wavelet projected onto the space curve at point $t=0$ on the space curve. In order to demonstrate more clearly and intuitively, local enlarged detail is shown in the second column graph of Fig. 7.

An numerical example is given for discussing the applications of local continuous wavelet transform and its reconstruction formula on a space curve $\vec{r}(t)$. Construct a local original signal $f(T)$ on the tangent line the space curve at point $t=0$ as follows:

$$f(T) = 0.2\sin(10T) + 0.1\cos(50T)$$

where $T \in [-0.5, 0.5]$. The local original signal $f(T)$ can be lifted onto the space curve by the projection of a space curve $\vec{r}(t)$ on the space curve in Sect. 2.2. The figures are shown in the Fig. 8. The space curve $\vec{r}(t)$ is shown by the blue curve in the first row and first column graph of Fig. 8. The original signal lifted on the space curve $\vec{r}(t)$ at point $t=0$ is shown by the yellow curve in the first row and first column graph of Fig. 8. The original signal on the space curve oscillates near point $t=0$. According to the Matlab program [15] of the continuous wavelet transform and its reconstruction formula discussed in Theorem 3.1, the reconstruction signal on the space curve $\vec{r}(t)$ at point $t=0$ is can be computed and shown by the yellow curve in the second row and first column graph of Fig. 8. In order to demonstrate more clearly and intuitively, local enlarged detail is shown in the second column graph of Fig. 8. The local original signal is shown by the yellow curve in the first row and second column graph of Fig. 8. The local space curve is shown by the blue curve in the first row and second column graph. The local reconstructed signal by CWT is shown by the yellow curve in the second row and second column graph of Fig. 8, compared to the blue space curve, which is the original signal. The norm of the error is 0.3783 between original signal and reconstructed signal.

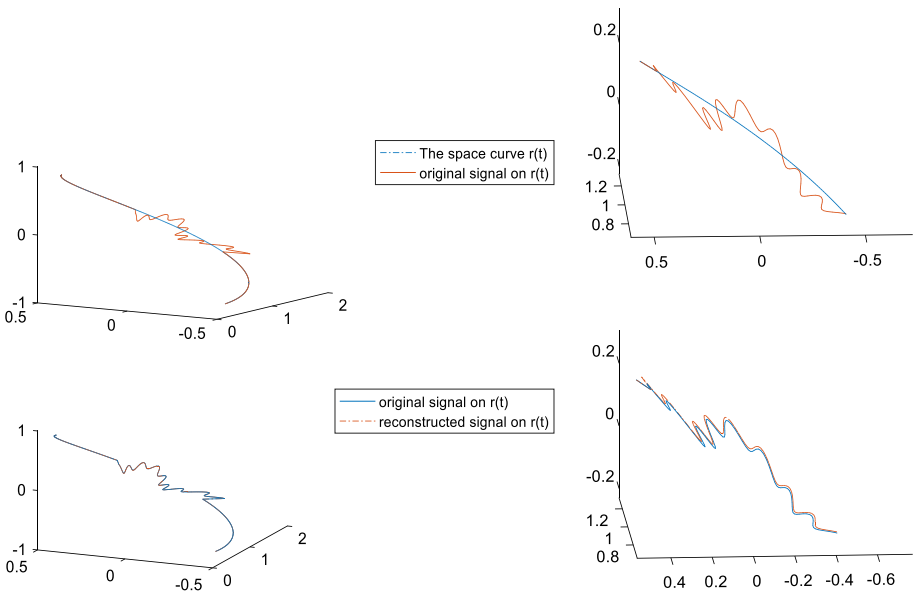

Fig. 8 Original signal and its reconstruction signal on the space curve

Example 5.2 Consider the wavelet 'Db3' in Refs. [5, 16]. The scaling function of 'Db3' wavelet satisfies the two-scale equation:

$$\begin{aligned}\phi(x) =& \frac{1+\sqrt{10}+\sqrt{5+2\sqrt{10}}}{16}\phi(2x)\\ &+\frac{5+\sqrt{10}+3\sqrt{5+2\sqrt{10}}}{16}\phi(2x-1)\\ &+\frac{10-2\sqrt{10}+2\sqrt{5+2\sqrt{10}}}{16}\phi(2x-2)\\ &+\frac{10-2\sqrt{10}-2\sqrt{5+2\sqrt{10}}}{16}\phi(2x-3)\\ &+\frac{5+\sqrt{10}-3\sqrt{5+2\sqrt{10}}}{16}\phi(2x-4)\\ &+\frac{10+\sqrt{10}-\sqrt{5+2\sqrt{10}}}{16}\phi(2x-5)\end{aligned}$$

and the wavelet function of 'Db3' wavelet satisfies

$$\begin{aligned}\psi(x) =& \frac{5+\sqrt{10}+3\sqrt{5+2\sqrt{10}}}{16}\phi(2x)-\frac{1+\sqrt{10}+\sqrt{5+2\sqrt{10}}}{16}\phi(2x-1)\\ &-\frac{10-2\sqrt{10}+2\sqrt{5+2\sqrt{10}}}{16}\phi(2x+1)+\frac{10-2\sqrt{10}-2\sqrt{5+2\sqrt{10}}}{16}\phi(2x+2)\\ &-\frac{5+\sqrt{10}-3\sqrt{5+2\sqrt{10}}}{16}\phi(2x+3)+\frac{1+\sqrt{10}-\sqrt{5+2\sqrt{10}}}{16}\phi(2x+4).\end{aligned}$$

According to the length-preserving projection on a circular helix in Sect. 2.2.2, the above scaling function ϕ and wavelet function ψ can be lifted onto a circular helix C. So the scaling function ϕ^C and wavelet function ψ^C can be deduced and the corresponding two-scale sequence can also be determined. According to Theorems 4.1 and 4.4, the two-scale equations of ϕ^C and ψ^C can be obtained by Eqs. (26) and (31) and given as follows:

$$\begin{aligned}\phi^C(\xi) =& \frac{1+\sqrt{10}+\sqrt{5+2\sqrt{10}}}{16}\phi^C\circ p^{-1}(2\cdot p(\xi))\\ &+\frac{5+\sqrt{10}+3\sqrt{5+2\sqrt{10}}}{16}\phi^C\circ p^{-1}(2\cdot p(\xi)-1)\\ &+\frac{10-2\sqrt{10}+2\sqrt{5+2\sqrt{10}}}{16}\phi^C\circ p^{-1}(2\cdot p(\xi)-2)\\ &+\frac{10-2\sqrt{10}-2\sqrt{5+2\sqrt{10}}}{16}\phi^C\circ p^{-1}(2\cdot p(\xi)-3)\\ &+\frac{5+\sqrt{10}-3\sqrt{5+2\sqrt{10}}}{16}\phi^C\circ p^{-1}(2\cdot p(\xi)-4)\\ &+\frac{10+\sqrt{10}-\sqrt{5+2\sqrt{10}}}{16}\phi^C\circ p^{-1}(2\cdot p(\xi)-5)\end{aligned}$$

and

$$\begin{aligned}\psi^C(\xi) = &\frac{5+\sqrt{10}+3\sqrt{5+2\sqrt{10}}}{16}\phi^C \circ p^{-1}(2\cdot p(\xi))\\ &-\frac{1+\sqrt{10}+\sqrt{5+2\sqrt{10}}}{16}\phi^C \circ p^{-1}(2\cdot p(\xi)-1)\\ &-\frac{10-2\sqrt{10}+2\sqrt{5+2\sqrt{10}}}{16}\phi^C \circ p^{-1}(2\cdot p(\xi)+1)\\ &+\frac{10-2\sqrt{10}-2\sqrt{5+2\sqrt{10}}}{16}\phi^C \circ p^{-1}(2\cdot p(\xi)+2)\\ &-\frac{5+\sqrt{10}-3\sqrt{5+2\sqrt{10}}}{16}\phi^C \circ p^{-1}(2\cdot p(\xi)+3)\\ &+\frac{1+\sqrt{10}-\sqrt{5+2\sqrt{10}}}{16}\phi^C \circ p^{-1}(2\cdot p(\xi)+4)\end{aligned}$$

where $p(\xi) = x$. According to the length-preserving projection on a circular helix curve C, the figure of the scaling function ϕ^C and wavelet ψ^C can be shown in Fig. 9, where the circular helix curve is in Sect. 2.

In first row of Fig. 9, scaling function ϕ of Db3 is given at left side and wavelet function ψ is shown at right side. The corresponding scaling function ϕ^C and wavelet function ψ^C on a circular helix curve are shown by the red curve at left side and right side of second row in Fig. 9, respectively.

Consider an original signal $f(t)$ as follows:

$$f(t) = 0.5\sin(10t) + 0.2\varepsilon_t$$

where $\varepsilon_t \sim N(0, \sigma^2)$. And the length of a part of the circular helix curve is 60. The original signal is generated onto the circular helix curve by lifting onto the circular helix curve. The circular helix curve is shown in the first row of Fig. 10 and the original signal on the circular helix curve is also shown by the red dotted line in the first row of Fig. 10. According to wavelet "db3" lifted onto the circular helix curve C, the original

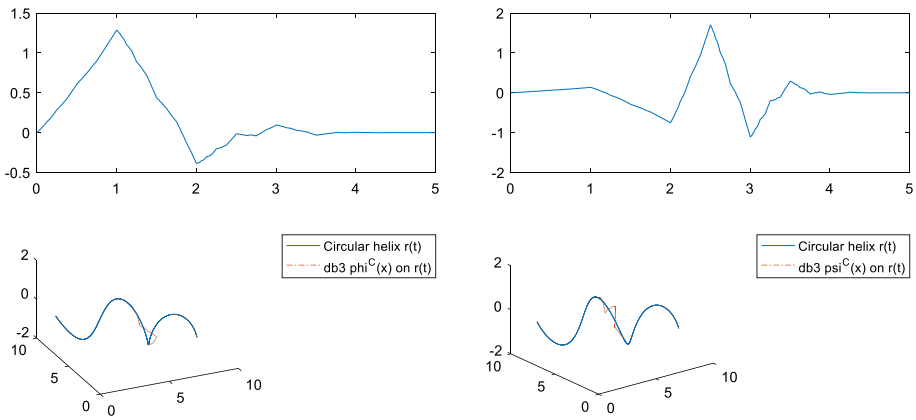

Fig. 9 Figures of scaling function ϕ^C and wavelet ψ^C on a circular helix curve

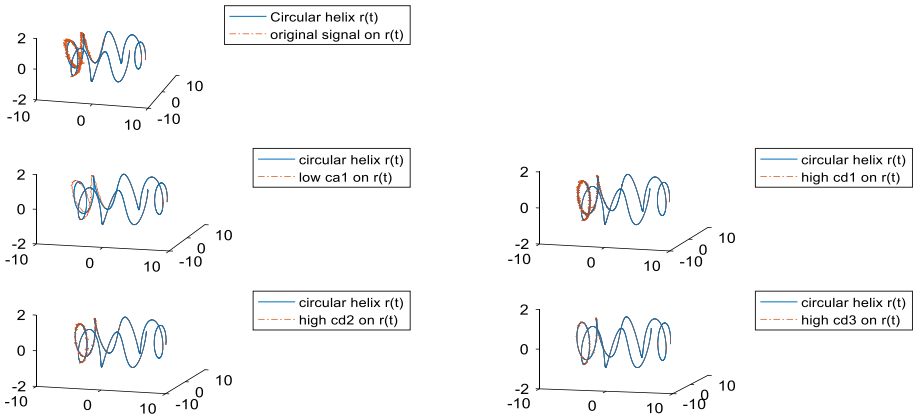

Fig.10 Original signal on the circular helix curve and its decomposition

signal on the circular helix curve can be decomposed to scale 3 on a scale-by-scale basis by decomposition and reconstruction on a helix space curve in Sect. 4. Low frequency signal ca1, high frequency signals cd1, cd2 and cd3 can be obtained. In the second row of Fig. 10, the low frequency signal ca1 is given and it captures the main approximate signal of the original signal on the circular helix curve. In Fig. 10, the high frequency signals cd1, cd2 and cd3 are also given and they capture the detailed information of the original signal with the circular helix curve, according to different scales. By the length-preserving projection, the circular helix curve can be flatten. Moreover, original signal and its decomposition on a circular helix curve can also be flatten for the comparison.

By reconstruction algorithm and length-preserving projection, the low-frequency signal ca1, high-frequency signal cd1, cd2 and cd3 can be reconstructed to obtain the reconstructed signal. It is shown in the second row graph of Fig. 11, compared to the original signal in the first row graph of Fig. 11. And the error signal is also shown in the third row of Fig. 11. The norm of error is 8.0741×10^{-11} between original signal and reconstructed signal.

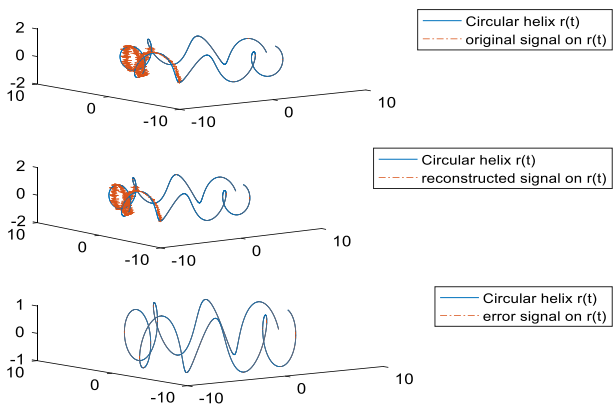

Fig. 11 Original signal, reconstructed signal on a circular helix curve and its error signal

6 Discussion and conclusion

In this paper, wavelet analysis on a class of helix space curves is discussed, including of local continuous wavelet transform at some point and discrete wavelet transform on a class of helix curves. Based on the tangent projection at some point from a space curve on the unit sphere onto its tangent line, local continuous wavelet transform and its reconstruction formula are deduced at some point of a space curve on the unit sphere. Moreover, an example is given for illustrating the application of local continuous wavelet transform at some point of a space curve, such as Example 5.1. According to the discretization of length-preserving projection and orthogonal multi-resolution analysis on a space curve, discrete wavelet transform is lifted onto a helix space curve, such as a circular helix curve. Based on length-preserving projection, the some properties, such as two-scale sequences of scaling function and wavelet, orthogonality, decomposition formula and so on, are discussed. Some results are are similar to the formula about the traditional wavelet transform. Moreover, an example and figures are given for illustrating wavelet function and discrete wavelet transform on a circular helix curve. Finally, an numerical example is given for decomposing and reconstructing with the signal on a circular helix curve.

Both local wavelet transform on a space curve on the unit sphere and discrete wavelet transform a helix space curve implicate a new wavelet method for dealing with a signal on a space curve. Local continuous wavelet transform on a space curve on the unit sphere is a method for processing the data on a space curve locally. The points of the neighborhood $B_{(\xi 0)}$ is projected onto the tangent line at point ξ_0 and then the dilated and translated points are pulled back onto the space curve by the tangent projection. Its adjacent structure is beneficial for exploring local approximate wavelet approaches. It is also a local approximation method of projecting the data to the tangent line. Discrete wavelet transform a helix space curve is another method for processing the data on a helix space curve. This method is based on the Euler discretization scheme of length-preserving projection. A helix space curve with length L can be projected onto a straight line with the same length by the discretized length-preserving projection p. In the other word, by the discretized inverse projection p^{-1}, every point on the straight line with length L can be lifted onto the corresponding point on a helix space curve. It is also approximation method and more convenient in computing inner product and wavelet transform. In Example 5.1, the norm of the error is 0.3783 between original signal and reconstructed signal. And the norm of error is 8.0741×10^{-11} in Example 5.2. The error by discrete wavelet transform based on Euler discretization scheme of length-preserving projection is much smaller than that by local continuous wavelet transform based on tangent projection. These have a new inspiration for dealing with some data on a space curves, such as satellite running data on its orbit. These may also provide an idea to estimate the orbit of celestial objects through local observational data. We will do a further discussion in our follow up study.

Author contributions
Xiaohui Zhou wrote the main manuscript and prepared all figures.

Funding
Not applicable.

Data availability
No, I do not have any research data outside the submitted manuscript file.

Declarations

Competing interests
The authors declare that they have no competing interests.

Received: 13 April 2024 Accepted: 6 June 2024
Published online: 14 June 2024

References

1. X. Zhou, B. Wang, Wavelet analysis on some smooth surface with nonzero constant Gaussian curvature. Int. J. Wavelets Multiresolut. Inf. Process. **16**(1), 1850007 (2018)
2. X. You, Q. Li, D. Tao, W. Ou, M. Gong, Local metric learning for exemplar-based object detection. IEEE Trans. Circuits Syst. Video Technol. **24**, 1265–1276 (2014)
3. D. Zhang, X. You, P. Wang, S.N. Yanushkevich, Y.Y. Tang, Facial Biometrics using non-tensor productwavelet and 2D discriminant techniques. Int. J. Pattern Recognit. Artif. Intell. **23**(3), 1–21 (2009)
4. F. In, S. Kim, *An Instruction to Wavelet Theory in Finance: A Wavelet Multiscale Approach* (World Scientific, Singapore, 2012)
5. X. Zhou, Wavelet transform on regression trend curve and its application in financial data. Int. J. Wavelets Multiresolut. Inf. Process. **18**(6), 2050040 (2020)
6. X. Zhou, G. Wang, Biorthogonal wavelet on a logarithm curve. J. Math. **2021**, 7985069 (2021)
7. A.K. Singh, H. Bhate, Stochastic wavelets from minimizers of an uncertainty principle: an example. Int. J. Wavelets Multiresolut. Inf. Process. **18**, 2050046 (2020)
8. J.P. Leduc, Spatiotemporal wavelet transforms for digital signal analysis. Signal Process. **60**(1), 23–41 (1997)
9. K. Kikuchi, B. Wang, Spatiotemporal wavelet transform and the multiscale behavior of the Madden–Julian oscillation. J. Clim. Am. Meteorol. Soc. **23**, 3814–3834 (2010)
10. F. Mujica, J.P. Leduc, M.J.T. Smith, R. Murenzi, SpatioTemporal wavelets: a group-theoretic construction for motion estimation and tracking. SIAM J. Appl. Math. **61**(2), 596–632 (2000)
11. F. Mujica, J.P. Leduc, M.J.T. Smith, R. Murenzi, Spatiotemporal continuous wavelets applied to missile warhead detection and tracking, in *Proceedings of Visual Communications Image Processing*, vol. 3024 (San Jose, California, 1997)
12. J.-P. Antoine, R. Daniela, P. Vandergheynst, Wavelet transform on manifolds: old and new approaches. Appl. Comput. Harmon. Anal. **28**, 189–202 (2010)
13. D. Rosca, Wavelet analysis on some surfaces of revolution via area preserving projection. Appl. Comput. Harmon. Anal. **30**(2), 262–272 (2011)
14. B.-Q. Wang, G. Wang, X.-H. Zhou, Y. Su, Wavelet analysis on developable surface on area-preserving projection. Int. J. Wavelets Multiresolut. Inf. Process. **13**(1), 1550007 (2015)
15. J. Erickson, Continuous wavelet transform and inverse (https://www.mathworks.com/ matlabcentral/fileexchange/20821-continuous-wavelet-transform-and-inverse), MATLAB Central File Exchange. Retrieved May 1, 2022 (2022).
16. D.I. Ten, *Lectures on Wavelets* (PASIAM Press, Philadelphia, 1992)
17. M. Dadkhah, R. Kamgar, H. Heidarzadeh, Reducing the cost of calculations for incremental dynamic analysis of building structures using the discrete wavelet transform. J. Earthq. Eng. **26**(7), 3317–3342 (2022)
18. R. Kamgar, M. Dadkhah, H. Naderpour, Seismic response evaluation of structures using discrete wavelet transform through linear analysis. Structures **29**, 863–882 (2021)
19. R. Kamgar, M. Dadkhah, H. Naderpour, Earthquake-induced nonlinear dynamic response assessment of structures in terms of discrete wavelet transform. Structures **39**, 821–847 (2022)
20. A. Heidari, J. Raeisi, R. Kamgar, Application of wavelet theory with denoising to estimate the parameters of an earthquake. Scientia Iranica A **28**(1), 49–64 (2021)
21. B.Q. Wang et al., A local wavelet transform on the torus T2. Int. J. Wavelets Multiresolut. Inf. Process. **13**, 1550027 (2015)
22. B. Wang, G. Wang, X. Zhou, Construction of the multi-wavelets on some smooth plane curves via length-preserving projection. Int. J. Wavelets Multiresolut. Inf. Process. **12**(01), 1450005 (2014)
23. S.G. Mallat, A theory for multiresolution signal decomposition: the wavelet representation. IEEE Trans. Pattern Anal. Mach. Intell. **11**, 674–693 (1989)
24. E. Guariglia, S. Silvestrov, Fractional-wavelet analysis of positive definite distributions and wavelets on D′(C), in *Engineering Mathematics II*, ed. by S. Silvestrov, M. Rancic (2016), p. 337–353
25. L. Yang, H. Su, C. Zhong et al., Hyperspectral image classification using wavelet transform- based smooth ordering. Int. J. Wavelets Multiresolut. Inf. Process. **17**(6), 1950050 (2019)
26. E. Guariglia, R.C. Guido, Chebyshev wavelet analysis. J. Funct. Spaces **1**, 5542054 (2022)
27. X. Zheng, Y.Y. Tang, J. Zhou, A framework of adaptive multiscale wavelet decomposition for signals on undirected graphs. IEEE Trans. Signal Process. **67**(7), 1696–1711 (2019)
28. E. Guariglia, Primality, fractality and image analysis. Entropy **21**(3), 304 (2019)
29. M.V. Berry, Z.V. Lewis, On the Weierstrass–Mandelbrot fractal function. Proc. R. Soc. Lond. Ser. A **370**(1743), 459–484 (1980)

Publisher's Note